Auditory circuit in the *Drosophila* brain

Jason Sih-Yu Lai[a], Shih-Jie Lo[a], Barry J. Dickson[b], and Ann-Shyn Chiang[a,c,d,e,1]

[a]Institute of Biotechnology and Department of Life Science, National Tsing Hua University, Hsinchu 30013, Taiwan; [b]Institute of Molecular Pathology, A-1030 Vienna, Austria; [c]Brain Research Center, National Tsing Hua University, Hsinchu 30013, Taiwan; [d]Genomics Research Center, Academia Sinica, Nankang, Taipei 11529, Taiwan; and [e]Kavli Institute for Brain and Mind, University of California at San Diego, La Jolla, CA 92093

Edited by Barry Ganetzky, University of Wisconsin, Madison, WI, and approved December 31, 2011 (received for review October 20, 2011)

Most animals exhibit innate auditory behaviors driven by genetically hardwired neural circuits. In *Drosophila*, acoustic information is relayed by Johnston organ neurons from the antenna to the antennal mechanosensory and motor center (AMMC) in the brain. Here, by using structural connectivity analysis, we identified five distinct types of auditory projection neurons (PNs) interconnecting the AMMC, inferior ventrolateral protocerebrum (IVLP), and ventrolateral protocerebrum (VLP) regions of the central brain. These auditory PNs are also functionally distinct; AMMC-B1a, AMMC-B1b, and AMMC-A2 neurons differ in their responses to sound (i.e., they are narrowly tuned or broadly tuned); one type of audioresponsive IVLP commissural PN connecting the two hemispheres is GABAergic; and one type of IVLP-VLP PN acts as a generalist responding to all tested audio frequencies. Our findings delineate an auditory processing pathway involving AMMC→IVLP→VLP in the *Drosophila* brain.

calcium imaging | FlyCircuit | GFP reconstitution across synaptic partners | polarity

Auditory systems are critical to the behavior of many insects. In *Drosophila melanogaster*, acoustic communication is essential for making decisions related to mate selection (1–4). During courtship, male flies flap one wing to produce a complex pattern of airborne vibrations comprising sine song and pulse song (5, 6). The pulse song enables the female to determine whether her suitor is of the same species (7). Courting males also monitor their own sounds to fine tune the courtship song (8). The courtship song is detected by auditory sensory neurons linking the Johnston organ (JO) at the second antennal segment to the antennal mechanosensory and motor center (AMMC) zones AB in the brain (9–12). It has been shown that the transient receptor potential vanilloid channels (Inactive and Nanchung) and a no mechanoreceptor potential C TRP channel expressed in JO-AB neurons are essential for normal acoustic transduction (13–16).

Four different projection neurons (PNs) innervating the AMMC zones AB have been reported based on *Gal4* expression patterns (12). The giant fiber neuron links AMMC zone A to the inferior ventrolateral protocerebrum (IVLP; a brain region defined by immunostaining of synaptic proteins) and thoracic ganglia; AMMC-A1 neuron connects AMMC zone A and the IVLP; AMMC-B1 neuron links AMMC zone B to the IVLP; and AMMC-B2 neurons are commissural neurons connecting AMMC zone B in both hemispheres. The intense innervations of the IVLP suggest that the IVLP functions as a second-level auditory processing center (12). More recently, stochastic labeling of 16,000 single neurons in the entire fly brain revealed that many AMMC PNs terminate at the caudoventrolateral protocerebrum (CVLP; a brain region analogous to IVLP and defined by clustered local neurons) (17), suggesting that the IVLP/CVLP region may be involved in auditory functions. However, a structural and functional map of cell-to-cell connectivity is first required to determine the direction of information flow, and to understand how auditory signals are represented and processed in the brain to orchestrate corresponding behaviors. In this study, we combined neural tracing with photoactivatable GFP (PaGFP) and visualized physical contact between neurons with GFP reconstitution across synaptic partners (GRASP) to construct a map of structural connections among the AMMC, IVLP, and ventrolateral protocerebrum (VLP). Moreover, the directions of information flow in this map were determined by polarity analysis and functional imaging.

Results

Brain Centers Processing Auditory Information. We started by identifying the major AMMC neural tracts by using PaGFP expression in living flies in which *Cha-Gal4* drives the expression of *UAS-PaGFP* and *UAS-mKO* in approximately 60% of the total brain neurons (17, 18). By using Monomeric Kusabira Orange (mKO) fluorescence to identify brain structures, we photoactivated the PaGFP in a 3D region of interest with a two-photon laser to localize the 810-nm light with submicrometer precision (19). This procedure allowed us to trace all Cha^+ fibers linking to the region of interest by anterograde and retrograde diffusion of the activated PaGFP molecules. We found that a single bundle of Cha^+ fibers linked the photoactivated AMMC region to the two IVLP regions in both brain hemispheres (Fig. 1*A*), similar to the morphology of the AMMC-B1 neurons (12). We then performed localized photoactivation at the IVLP. Consistent with the previous finding, Cha^+ fibers formed bundles linking the photoactivated IVLP region to the contralateral IVLP and the two AMMC regions in both brain hemispheres. An additional ascending neural tract linking ipsilateral IVLP and VLP was also identified (Fig. 1*B*). By using the 3D reconstruction of the standard brain model in the FlyCircuit database (17), spatial relationships between the PaGFP traced tracts were illustrated (Fig. 1*C*). Note that the VLP region in FlyCircuit is analogous to the brain region of AVLP plus PVLP in the Flybrain Neuron Database (20). These results lead to the conclusion that the AMMC-B1 neurons are the major second-level neurons, and a cluster of third-level neurons connecting the IVLP to the VLP was additionally revealed (Fig. 1*C*).

To determine whether Cha^+ neurons in the AMMC and IVLP were responsive to acoustic stimuli, we performed functional imaging by using a genetically encoded calcium sensor GCaMP1.6 driven by *Cha-Gal4* (21). A calcium wave in response to all test sound frequencies (100 Hz, 300 Hz, 700 Hz, and pulse song) was observed in the Cha^+ neurons of the AMMC and IVLP but not the antennal lobe (AL; Fig. S1 *A–C*). In the control experiment, GCaMP activation in response to an odorant (3-octanol) was observed in the AL but not the AMMC and IVLP.

AMMC-B1 Neurons. Because the AMMC-B1 neurons are likely the major second-level neurons in the *Drosophila* auditory system, we questioned whether these AMMC-B1 neurons could be further divided into different subtypes based on their functional responses or morphologies. By examining expression patterns of 4945 *Gal4* drivers, we obtained 10 drivers with preferential expression

Author contributions: J.S.-Y.L. and A.-S.C. designed research; J.S.-Y.L. and S.-J.L. performed research; B.J.D. contributed new reagents/analytic tools; J.S.-Y.L. and S.-J.L. analyzed data; and J.S.-Y.L. and A.-S.C. wrote the paper.

The authors declare no conflict of interest.

This article is a PNAS Direct Submission.

[1]To whom correspondence should be addressed. E-mail: aschiang@life.nthu.edu.tw.

This article contains supporting information online at www.pnas.org/lookup/suppl/doi:10.1073/pnas.1117307109/-/DCSupplemental.

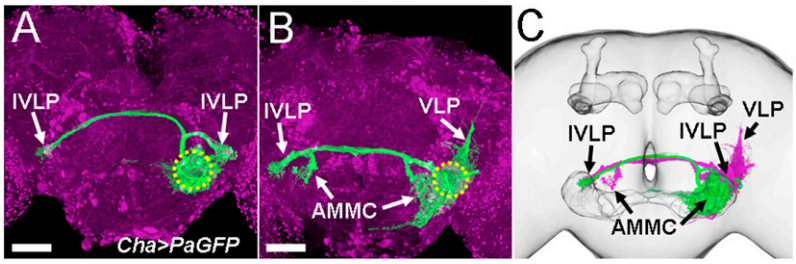

Fig. 1. Mapping auditory pathways with PaGFP photoactivation. (*A*) Anterior view of *Cha*$^+$ fibers linking AMMC regions. Photoactivation in one AMMC (dashed circle) labeled neural tracts (green) terminating at the two IVLPs. Magenta, mKO. Genotype: *Cha-Gal4/UAS-mKO,UAS-mKO;UAS-PaGFP*. (*B*) Anterior view of *Cha*+ fibers linking IVLPs. Photoactivation in one IVLP (dashed circle) labeled neural tracts (green) terminating in the contralateral IVLP, both the AMMCs, and the ipsilateral VLPs. Magenta, mKO. Genotype: *Cha-Gal4/UAS-mKO,UAS-mKO;UAS-PaGFP*. (*C*) Three-dimensional reconstruction of neural tracts, traced by photoactivation in AMMC (green) and IVLP (magenta), in the standard brain. (Scale bars, 50 μm.)

in the AMMC-B1 neurons (Fig. 2*A*). Functional imaging of the IVLP region showed that all these AMMC-B1 neurons exhibited GCaMP activation in response to acoustic stimuli (Fig. 2*B*). In total, we observed four different combinations of responses to 100 Hz, 300 Hz, 700 Hz, and pulse song stimuli. Type I (*E0564*, *E0583*, *VT27938*, and *VT19992*) was narrowly tuned for sensing low frequency of 100 Hz only. Type II (*VT10277*, *VT45599*, and *VT20611*) responded to 100 Hz and 300 Hz, but not 700 Hz or pulse song. Type III (*VT26006*, *GH86*) responded to 100 Hz, 300 Hz, and pulse song, but not 700 Hz. Type IV (*VT30609*) was broadly tuned for sensing all tested frequencies.

VT30609-Gal4 was expressed in two separate AMMC neural tracts, suggesting that this driver may contain more than just AMMC-B1 neurons (Fig. 2). By using flip-out labeling to visualize individual neurons (22), we found that *VT30609-Gal4* also contained AMMC-A2 neurons that projected bilaterally via a ventral neural tract to extend dendrites into AMMC zone A in both hemispheres and axonal terminals in the ipsilateral IVLP (Fig. 2 and Fig. S2*B*). Monitoring the GCaMP activation of AMMC-A2 neurons in the ventral neural tract to avoid interference from the AMMC-B1 neurons, we found that the AMMC-A2 neurons exhibited broadly tuned sensitivity to all tested frequencies (Fig. S3 and Table S1). Single-cell imaging revealed that, regardless of functional diversity, the AMMC-B1 neurons were isomorphic in all 5 *Gal4* lines examined (Fig. S2*A*): *E0564-Gal4* (9 ± 4 neurons, $n = 15$), *E0583-Gal4* (11 ± 4 neurons, $n = 10$), *VT45599-Gal4* (10 ± 2 neurons, $n = 5$), *VT26006-Gal4* (6 ± 1 neurons, $n = 5$), and *VT30609-Gal4* (9 ± 2 neurons, $n = 15$).

To elucidate the direction of information flow, we used Dscam::GFP as a dendrite marker (23) and synaptotagmin (syt):: GFP as an axon terminal marker (24) to unravel the polarity of AMMC PNs. In all cases, we found that Dscam::GFP signals were located in the AMMC and syt::GFP signals were located in the IVLP (Fig. 2*C*). Thus, these AMMC-B1 neurons and AMMC-A2 neurons likely receive and relay auditory information from the AMMC to the IVLP.

Next, we used GRASP (25) to test whether these isomorphic AMMC-B1 neurons connected to distinct types of JO neurons. We used *L5219-LexA* expressed in a small subset of JO neurons to drive *lexAop-spGFP*$_{11}$, and various *Gal4s* expressed in AMMC-B1 neurons to drive *UAS-spGFP*$_{1–10}$ (Fig. S4*A*). When paired with *L5219-LexA*, GRASP signals were observed in the AMMC in *VT45599-*, *VT26006-* and *VT30609-Gal4s* (Fig. S4 *B–D*), but not in *E0564-* and *E0583-Gal4s* (Fig. S4 *E* and *F*). These results indicate that AMMC-B1 neurons with diverse auditory responses and JO connectivities can be further classified into two subtypes: AMMC-B1a (in *E0564-* and *E0583-Gal4s*), which are narrowly tuned for sensing only 100 Hz stimulus, and AMMC-B1b (in *VT45599-*, *VT26006-*, and *VT30609-Gal4s*), which are more broadly tuned for sensing 100-Hz and 300-Hz but not 700-Hz stimuli (Table S1).

IVLP-IVLP PNs. We next examined commissural PNs linking the left and right IVLPs in *VT50245-Gal4* (Fig. 3*A*). Single-cell imaging with flip-out labeling indicated that *VT50245-Gal4* contained IVLP-IVLP PNs with cell bodies located in the ventral-medial subesophageal region and sending bilateral projections to both IVLPs (Fig. 3*B*). Immunolabeling of *VT50245-Gal4* neurons showed that the IVLP-IVLP PNs, but not their neighboring cells or olfactory PNs, were anti-GABA immunopositive (Fig. 3*C* and Fig. S5). These IVLP-IVLP neurons were immunonegative for antibodies against vesicular glutamate transporter and serotonin (Fig. S5). Polarity analysis showed strong Dscam::GFP and syt:: GFP signals in both IVLPs (Fig. 3*D*). To examine structural connections, we used *L5055-LexA*-containing AMMC-B1 neurons for two-color labeling and GRASP analysis (Fig. S6*A*). We first examined whether AMMC-B1 neurons in *L5055-LexA* were directly connected to *nan-Gal4* neurons that include most if not all JO neurons and innervate all AMMC zones (Fig. S6*B*) (12). Positive GRASP signals between *L5055-LexA* and *nan-Gal4* neurons were detected in the AMMC (Fig. S6*C*). These *L5055-LexA* neurons belonged to the AMMC-B1b neurons because they responded to 100-Hz and 300-Hz stimuli and pulse song, but not 700-Hz stimuli (Fig. S6*D*). Direct connections between AMMC-B1b neurons and IVLP-IVLP PNs in the IVLP were observed by two-color labeling (Fig. 3*E*, *Inset*), and GRASP signals (Fig. 3*E*). Consistently, functional imaging also indicated that these IVLP-IVLP PNs were responsive to 100 Hz and 300 Hz stimuli and pulse song, but not 700 Hz stimuli (Fig. 3*F*).

IVLP-VLP PNs. PaGFP photoactivation revealed a short neural tract projecting dorsally from the IVLP to a small region in the VLP. By analyzing the expression patterns of 4945 *Gal4* drivers, we found that *VT34811-Gal4* was specifically expressed in a cluster of neurons with cell bodies located between the optic lobe and the central brain, sending extensive fibers to the IVLP and a short neural tract projecting dorsally to the VLP (Fig. 4*A*). Single-cell imaging with flip-out labeling confirmed that *VT34811-Gal4* contained only one type of IVLP-VLP PN (Fig. 4*B*). These IVLP-VLP PNs had putative dendrites labeled by Dscam::GFP in the IVLP and axons labeled by syt::GFP in the VLP (Fig. 4*C*). Two-color labeling showed extensive intersections between dendrites (magenta) of the IVLP-VLP PNs and axonal terminals (green) of the AMMC-B1 neurons in the IVLP (Fig. 4*D*, *Inset*). Intense GRASP signals confirmed direct structural connections between the AMMC-B1 neurons and IVLP-VLP PNs (Fig. 4*D*). Interestingly, functional imaging showed that these IVLP-VLP PNs were auditory generalists responsive to all tested acoustic stimuli (Fig. 4*E*). Thus, the broadly tuned IVLP-VLP PNs likely receive signals from more than just AMMC-B1 neurons.

Other Putative Auditory Circuits. We classified the auditory circuit based on limited numbers of *Gal4* lines by using PaGFP tracing,

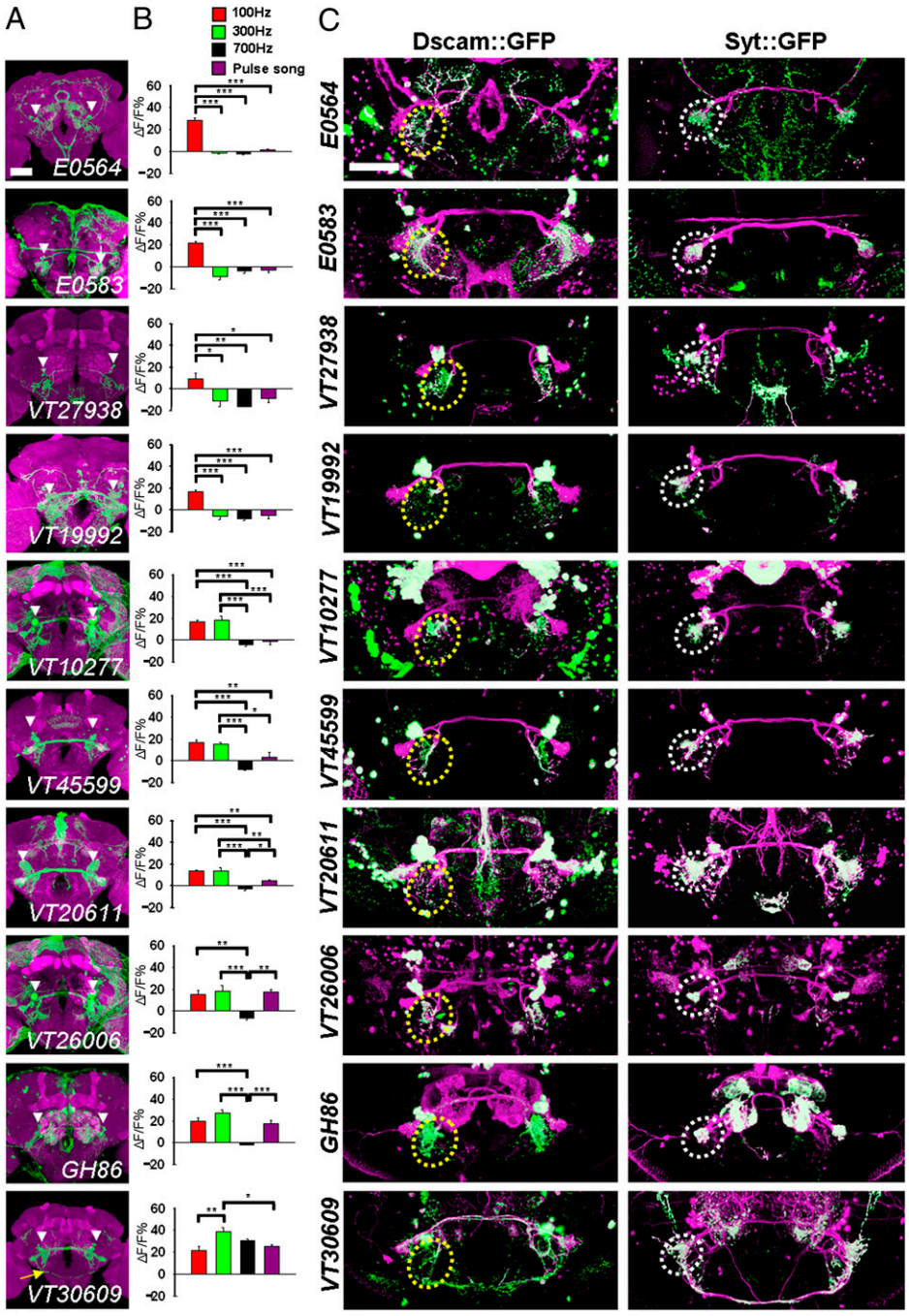

Fig. 2. Four types of auditory responses from AMMC PNs. (*A*) *Gal4* expression patterns reported by *UAS-mCD8::GFP* (green) in the brain immunostained with anti-Discs large (DLG) antibody (magenta). *VT30609-Gal4* contains a ventral tract (arrow) that is not in the other drivers. Arrowheads denote cell bodies. (*B*) Calcium responses in the IVLP in *Gal4s>UAS-GCaMP1.6* flies. Each value represents mean ± SEM (n = 5–8) for the ratio of peak amplitudes before and after acoustic stimuli (ΔF/F%; *$P < 0.05$, **$P < 0.01$, and ***$P < 0.001$). (*C*) Axon-dendrite polarity analysis in *Gal4s>UAS-Dscam::GFP;UAS-mKO* and *Gal4s>UAS-syt::GFP;UAS-mKO* flies. In all cases, AMMC PNs project Dscam fibers into the AMMC (yellow dotted circle) and synaptotagmin fibers into the IVLP (white dotted circle). Green, GFP; magenta, mKO. (Scale bars, 50 μm.)

single-cell labeling, and functional imaging. To assess the completeness of this map, we examined the FlyCircuit database for putative auditory neurons innervating the AMMC or CVLP (17). Eight additional candidate auditory neurons were identified (Fig. S7). Although further functional studies are needed, most of the AMMC PNs connect to the contralateral AMMC or the IVLP/CVLP, supporting the previous prediction that IVLP/CVLP is the major second-level auditory processing center (12, 17).

Discussion

Our findings point to a model in which a central pathway relays auditory information from the AMMC zones AB to the two IVLPs and then to the ipsilateral VLP (Fig. 5). This conclusion is supported by three independent lines of evidence from structural and functional characterization of the involved neurons. First, polarities of all involved neurons are consistent with the proposed direction of auditory information flow. The AMMC-B1

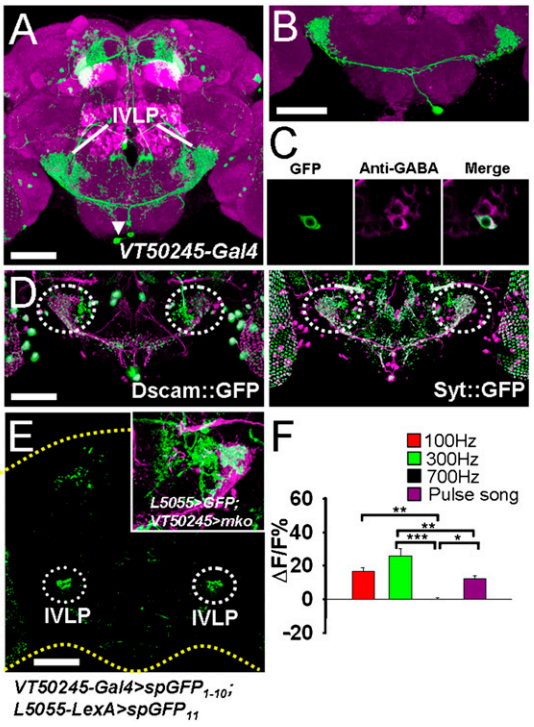

Fig. 3. Structural and functional characterization of IVLP-IVLP PNs. (*A*) The *VT50245-Gal4>UAS-mCD8::GFP* expression pattern (green) in the brain counterstained with anti-DLG antibody (magenta). Arrowhead denotes cell bodies. (*B*) Flip-out labeling of a single IVLP-IVLP PN. Genotype: *hs-flp; VT50245-Gal4/UAS>rCD2,y+>UAS-mCD8::GFP*. (*C*) The IVLP-IVLP PN from flip-out labeling (*hs-flp;VT50245-Gal4/UAS>rCD2,y+>UAS-mCD8::GFP*) are GABAergic. (*D*) Polarity analysis. *VT50245-Gal4>UAS-Dscam::GFP,UAS-mKO* showed dendritic *UAS-Dscam::GFP* marker (green) and *VT50245-Gal4>UAS-syt::GFP,UAS-mKO* showed axonal *UAS-syt::GFP* marker (green). *VT50245-Gal4* expression was reported by *UAS-mKO* (magenta). (*E*) GRASP-positive signals were detected between IVLP-IVLP PNs in *VT50245-Gal4>UAS-spGFP$_{1-10}$* and AMMC-B1 neurons in *L5055-LexA>LexAop-spGFP$_{11}$*. *Inset*: Two-color imaging of *L5055-LexA>lexAop-rCD2::GFP* (green) and *VT50245-Gal4>UAS-mKO* (magenta) in IVLP. White dots approximately outline the two IVLPs. Yellow dots outline the brain boundary. (*F*) Functional responses of IVLP to different audio frequencies in *VT50245-Gal4>UAS-GaMP 1.6* flies. Each value represents mean ± SEM (n = 5–7; *P < 0.05, **P < 0.01, and ***P < 0.001). (Scale bars, 50 μm.)

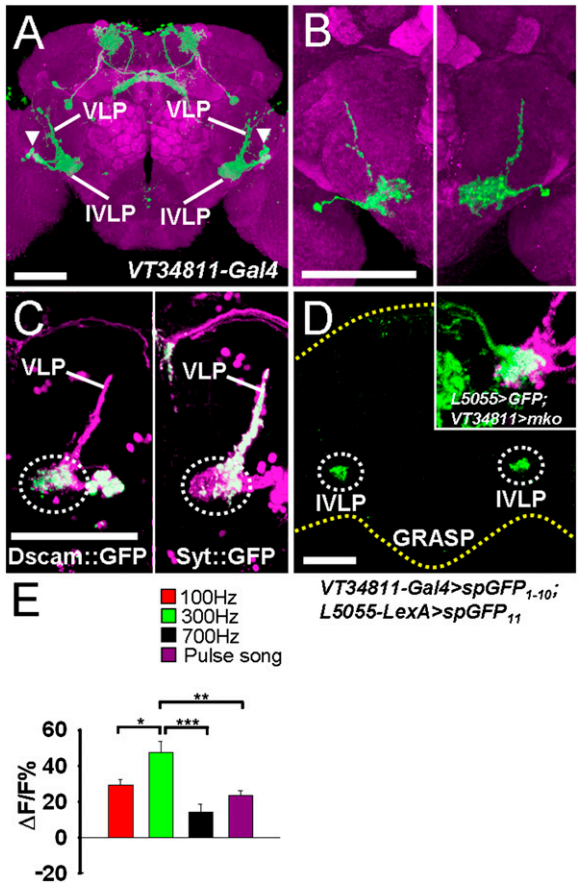

Fig. 4. Structural and functional characterization of IVLP-VLP PNs. (*A*) The *VT34811-Gal4>UAS-mCD8::GFP* expression pattern (green) in the brain counterstained with anti-DLG antibody (magenta). Arrowhead denotes cell bodies. (*B*) Flip-out labeling of two single IVLP-VLP PNs, one in each brain hemisphere. Genotype: *hs-flp;VT34811-Gal4/UAS>rCD2,y+>mCD8::GFP*. (*C*) Polarity analysis. *VT34811-Gal4>UAS-Dscam::GFP,UAS-mKO* showed dendritic *UAS-Dscam::GFP* marker (green) in the IVLP (*Left*) and *VT50245-Gal4>UAS-syt::GFP,UAS-mKO* showed axonal *UAS-syt::GFP* marker (green) in the VLP (*Right*). Magenta, mKO. White dots approximately outline the two IVLPs. (*D*) GRASP-positive signals were detected between AMMC-B1 neurons in *L5055-lexA>LexAop-spGFP$_{11}$* and IVLP-VLP PNs in the IVLP in *VT34811-Gal4>UAS-spGFP$_{1-10}$*. *Inset*: Two-color imaging of *L5055-LexA>LexAop-rCD2::GFP* (green) and *VT34811-Gal4>UAS-mKO* (magenta) in the IVLP. White dots approximately outline the two IVLPs. Yellow dots outline the brain boundary. (*E*) Functional responses of the IVLP to different audio frequencies in *VT34811-Gal4>UAS-GaMP1.6* flies. Each value represents mean ± SEM (n = 11; *P < 0.05, **P < 0.01, and ***P < 0.001). (Scale bars, 50 μm.)

neurons and AMMC-A2 neurons had their dendrites in the AMMC and axon terminals in the IVLP (Fig. 2*C*). The IVLP-IVLP PNs had both dendrites and axon terminals in both IVLPs (Fig. 3*D*). The IVLP-VLP PNs had dendrites in the IVLP and axons in the VLP (Fig. 4*C*). Second, two-color colocalization and GRASP visualization showed direct connections between JO neurons and AMMC-B1 neurons (Figs. S4 and S6), between AMMC-B1 neurons and IVLP-IVLP PNs (Fig. 3*E*), and between AMMC-B1 neurons and IVLP-VLP PNs (Fig. 4*D*). Third, all PNs in the proposed pathway were auditory-responsive. Taken together, we show that auditory information is processed by three consecutive brain centers: AMMC→IVLP→VLP.

In mammals, sound waves are transformed into vibrations of liquid in the cochlea. Each hair cell converts only particular frequencies of sound vibrations to neural signals in specific zones of the cochlea (26, 27). In flies, different frequencies of sound are detected by two groups of JO neurons (12). The JO-A neurons respond to a wide range of sound frequencies, and JO-B neurons are only sensitive to low frequencies. Consistent with these observations, we found different types of AMMC PNs processing specific ranges of sound frequencies (Fig. 2*B*). AMMC-B1a, AMMC-B1b, and AMMC-A2 neurons respond to 100 Hz, 100–300 Hz, and 100–700 Hz, respectively. Some but not all AMMC-B1b neurons also responded to pulse song, suggesting that additional subtypes of AMMC-B1 neurons may exist.

In contrast to the olfactory sensory neurons projecting to paired ALs in both brain hemispheres (28), JO neurons deliver auditory information only to the ipsilateral AMMC (29). Putative GABAergic AMMC-AMMC PNs found in the *Gad-Gal4* may be involved in an inhibitory function between the two AMMCs (Fig. S7). These audio signals then left the AMMC zones AB and projected into the IVLP via AMMC-B1 and AMMC-A2 neurons (Fig. 2 and Fig S2). A specific type of GABAergic commissural PNs innervates both IVLPs (Fig. 3). Further experiments are needed to determine if these GABAergic neurons in the auditory pathways modulate gain control similar to the GABAergic local neurons in the AL of the olfactory system (30).

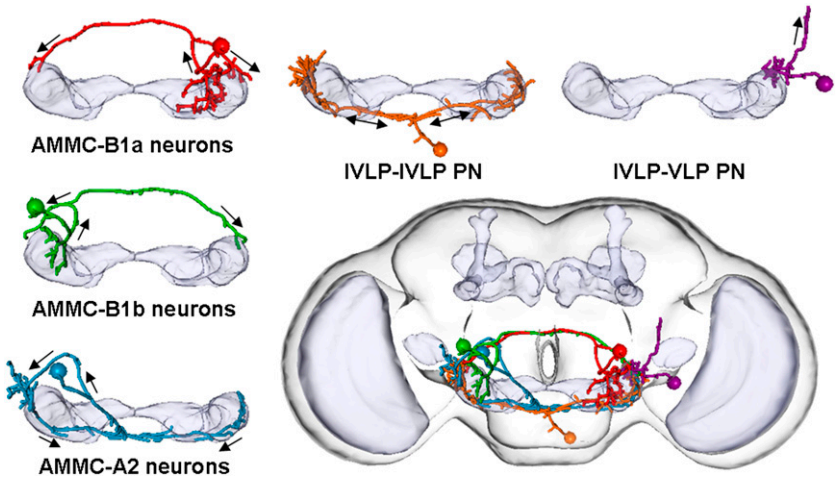

Fig. 5. Model of information flow in the *Drosophila* auditory system. Each color represents a distinct type of auditory responsive neuron. The skeleton was automatically traced using FlyCircuit. Arrows indicate the directions of auditory information flow.

At the third level of the auditory circuit, we found that only one type of IVLP-VLP PN responded to a wide range of sound frequencies (100–700 Hz). VLP is composed of glomerular structures that receive visual inputs from the lobula (31). A pheromone-sensing circuit that expresses Gr32a also targets the VLP (32). Furthermore, some JO neurons bypass AMMC to directly terminate at the ventrolateral brain (9), a neuropil region equivalent to CVLP plus VLP. Together, these findings suggest that VLP may act as a multimodality processing center to integrate visual, gustatory, and auditory information.

In conclusion, our findings establish a functional map of auditory circuits in the *Drosophila* brain. This auditory map suggests that narrowly and broadly tuned auditory reception by specific JO neurons are further represented in AMMC-B1a, AMMC-B1b, and AMMC-A2 neurons. Subsequent IVLP-VLP PNs then serve as generalists relaying all frequencies of auditory information to the VLP. These data form an essential foundation for further studies that will address the behavioral roles of these neurons, and explore how they are functionally integrated into the larger circuits that underlie these behaviors.

Materials and Methods

Fly Strains. Fly stocks were raised on standard cornmeal-yeast-agar medium at 25 °C and 60% to 70% relative humidity under a 12/12-h light/dark cycle. *E0564-Gal4* (w[*];P{w[+mW.hs]=GawB}Mmp2[NP0509]/CyO) was obtained from the *Drosophila* Genetic Resource Center (Kyoto, Japan). *E0583-Gal4* (w[1118];P{w[+mW.hs]=GawB}c135), *Cha-Gal4, UAS-syt::GFP*, and *UAS-mCD8::GFP* were obtained from Bloomington Stock Center (Bloomington, IN). *UAS-Dscam[17.1]::GFP* was from Tzumin Lee (Janelia Farm Research Campus, Howard Hughes Medical Institute, Ashburn, VA). CyO/*Sp;LexAop-spGFP*$_{11}$, *UAS-spGFP*$_{1-10}$ was from Kristin Scott (Department of Molecular & Cell Biology, University of California, Berkeley, CA). *UAS-GCaMP1.6* was from Dierk Reiff (Department for Neurobiology/Animal Physiology, University of Freiburg, Freiburg, Germany). *GH86-Gal4* was from Lei Liu (School of Life Science, Peking University, Beijing, China), and *hs-flp;*CyO/*Sp;UAS>rCD2, y+>mCD8::GFP* was from Richard Axel (Department of Neuroscience and the Howard Hughes Medical Institute, College of Physicians and Surgeons, Columbia University, New York, NY). *VT Gal4* lines were generated in the Dickson laboratory. The transgenic fly line *UAS-mKO* was generated in a Canton-S w^{1118} (iso1CJ) background by using standard techniques. *L5055-LexA* was generated by remobilization of *P{lexA-VP16.C}505* on the X chromosome (33). For single-neuron imaging, offsprings of *Gal4* lines crossed to *hs-flp;*CyO/*Sp;UAS>rCD2,y+>mCD8::GFP* were heat-shocked at 37 °C for 10 min at larval or pupal stage.

PaGFP Photoactivation. Living brains freshly dissected from flies carrying *Cha-Gal4/UAS-mKO,UAS-mKO;UAS-PaGFP* transgenes were mounted in PBS solution. Before photoactivation, PaGFP produced weak fluorescence when excited with a 488-nm laser. We used *UAS-mKO* expression (red) to define a volume of interest slightly smaller than the target neuropil region. Photoactivation was performed by scanning from the top to the bottom slices of the defined volume by using a two-photon laser of 820 nm. For photoactivation of PaGFP in AMMC and IVLP, one session was approximately 10 consecutive slices at 1-μm intervals. In total, we performed 100 sessions with a rest interval of 10 s between any two sessions to prevent overheating the sample. Next, sample brains were fixed in 4% paraformaldehyde (vol/vol) at room temperature for 10 min, degassed with vacuum in PBS solution containing 2% Triton-X 100 (vol/vol), and then mounted in FocusClear (CelExplorer) for confocal imaging.

Details of immunohistochemistry, image recording and processing, and calcium imaging are provided in *SI Materials and Methods*.

ACKNOWLEDGMENTS. We thank D. F. Reiff, Tzumin Lee, Kristin Scott, Lei Liu, Richard Axel, the *Drosophila* Genetic Resource Center, and the Bloomington Stock Center for providing transgenic flies. We thank Daniel F. Eberl for providing the *Drosophila* pulse song and Bryan Huang for comments on the manuscript. This work was supported by grants from the Ministry of Education and National Science Council (to A.-S.C.), the Human Frontier Science Programme, and the European Research Council (to B.J.D.).

1. Ewing B-C (1968) The courtship songs of Drosophila. *Behaviour* 31:288–301.
2. Von Schilcher F (1976) The role of auditory stimuli in the courtship of Drosophila melanogaster. *Anim Behav* 24:18–26.
3. Manoli DS, Meissner GW, Baker BS (2006) Blueprints for behavior: Genetic specification of neural circuitry for innate behaviors. *Trends Neurosci* 29:444–451.
4. Dickson BJ (2008) Wired for sex: The neurobiology of *Drosophila* mating decisions. *Science* 322:904–909.
5. Ejima A, Griffith LC (2008) Courtship initiation is stimulated by acoustic signals in *Drosophila melanogaster*. *PLoS ONE* 3:e3246.
6. Villella A, Hall JC (2008) Neurogenetics of courtship and mating in *Drosophila*. *Adv Genet* 62:67–184.
7. Eberl DF, Duyk GM, Perrimon N (1997) A genetic screen for mutations that disrupt an auditory response in *Drosophila melanogaster*. *Proc Natl Acad Sci USA* 94: 14837–14842.
8. Tauber E, Eberl DF (2001) Song production in auditory mutants of *Drosophila*: The role of sensory feedback. *J Comp Physiol A Neuroethol Sens Neural Behav Physiol* 187: 341–348.
9. Kamikouchi A, Shimada T, Ito K (2006) Comprehensive classification of the auditory sensory projections in the brain of the fruit fly *Drosophila melanogaster*. *J Comp Neurol* 499:317–356.
10. Kernan MJ (2007) Mechanotransduction and auditory transduction in *Drosophila*. *Pflugers Arch* 454:703–720.
11. Yorozu S, et al. (2009) Distinct sensory representations of wind and near-field sound in the *Drosophila* brain. *Nature* 458:201–205.
12. Kamikouchi A, et al. (2009) The neural basis of *Drosophila* gravity-sensing and hearing. *Nature* 458:165–171.
13. O'Neil RG, Heller S (2005) The mechanosensitive nature of TRPV channels. *Pflugers Arch* 451:193–203.

14. Todi SV, Franke JD, Kiehart DP, Eberl DF (2005) Myosin VIIA defects, which underlie the Usher 1B syndrome in humans, lead to deafness in *Drosophila*. *Curr Biol* 15:862–868.
15. Göpfert MC, Albert JT, Nadrowski B, Kamikouchi A (2006) Specification of auditory sensitivity by *Drosophila* TRP channels. *Nat Neurosci* 9:999–1000.
16. Todi SV, Sivan-Loukianova E, Jacobs JS, Kiehart DP, Eberl DF (2008) Myosin VIIA, important for human auditory function, is necessary for *Drosophila* auditory organ development. *PLoS ONE* 3:e2115.
17. Chiang AS, et al. (2011) Three-dimensional reconstruction of brain-wide wiring networks in *Drosophila* at single-cell resolution. *Curr Biol* 21:1–11.
18. Itoh N, et al. (1986) Cloning of *Drosophila* choline acetyltransferase cDNA. *Proc Natl Acad Sci USA* 83:4081–4085.
19. Testa I, et al. (2008) Spatial control of pa-GFP photoactivation in living cells. *J Microsc* 230:48–60.
20. Shinomiya K, Matsuda K, Oishi T, Otsuna H, Ito K (2011) Flybrain neuron database: a comprehensive database system of the *Drosophila* brain neurons. *J Comp Neurol* 519:807–833.
21. Reiff DF, et al. (2005) In vivo performance of genetically encoded indicators of neural activity in flies. *J Neurosci* 25:4766–4778.
22. Wong AM, Wang JW, Axel R (2002) Spatial representation of the glomerular map in the *Drosophila* protocerebrum. *Cell* 109:229–241.
23. Wang J, et al. (2004) Transmembrane/juxtamembrane domain-dependent Dscam distribution and function during mushroom body neuronal morphogenesis. *Neuron* 43:663–672.
24. Zhang YQ, Rodesch CK, Broadie K (2002) Living synaptic vesicle marker: Synaptotagmin-GFP. *Genesis* 34:142–145.
25. Gordon MD, Scott K (2009) Motor control in a *Drosophila* taste circuit. *Neuron* 61: 373–384.
26. Dallos P, Corey ME (1991) The role of outer hair cell motility in cochlear tuning. *Curr Opin Neurobiol* 1:215–220.
27. Ruggero MA (1992) Responses to sound of the basilar membrane of the mammalian cochlea. *Curr Opin Neurobiol* 2:449–456.
28. Rajashekar KP, Shamprasad VR (2004) Maxillary palp glomeruli and ipsilateral projections in the antennal lobe of *Drosophila melanogaster*. *J Biosci* 29:423–429.
29. Sivan-Loukianova E, Eberl DF (2005) Synaptic ultrastructure of *Drosophila* Johnston's organ axon terminals as revealed by an enhancer trap. *J Comp Neurol* 491: 46–55.
30. Wilson RI, Laurent G (2005) Role of GABAergic inhibition in shaping odor-evoked spatiotemporal patterns in the *Drosophila* antennal lobe. *J Neurosci* 25: 9069–9079.
31. Otsuna H, Ito K (2006) Systematic analysis of the visual projection neurons of *Drosophila melanogaster*. I. Lobula-specific pathways. *J Comp Neurol* 497:928–958.
32. Miyamoto T, Amrein H (2008) Suppression of male courtship by a *Drosophila* pheromone receptor. *Nat Neurosci* 11:874–876.
33. Lai SL, Lee T (2006) Genetic mosaic with dual binary transcriptional systems in *Drosophila*. *Nat Neurosci* 9:703–709.